

# Quantifying bead accumulation inside a cannibalistic macrophage population

Ryan J. Murphy, Adelle C.F. Coster, Jennifer A. Flegg, Joseph P. Ndenda, Mary R. Myerscough, and Helen M. Byrne

**Abstract** Macrophages are a key cell type in the immune system that can promote healing and disease progression. In this paper, we use statistical modelling to revisit the mathematical modelling and *in vitro* experiments of Ford et al. [1]. We focus on experiments that quantify the accumulation of latex beads in macrophages. This combined mathematical, statistical, and experimental approach provides a powerful framework to interpret and quantify fundamental macrophage processes, such as cell division, cell death, and the cannibalistic ingestion and removal of dead cells. We find that the previously reported estimate of a key mathematical model parameter obtained by visual inspection is not contained within the corresponding confidence interval obtained using our objective statistical modelling. We also explore how uncertainty in parameter estimates influences key predictions, such as the distribution of the number of beads per cell. This analysis provides a platform for future studies exploring substance accumulation in macrophage populations.

---

Ryan J. Murphy

UniSA STEM, The University of South Australia, Mawson Lakes, SA 5095, Australia  
e-mail: ryan.murphy@unisa.edu.au

Jennifer A. Flegg

School of Mathematics and Statistics, The University of Melbourne, Parkville, Victoria, Australia  
e-mail: ryan.murphy@unimelb.edu.au

Adelle C.F. Coster

School of Mathematics and Statistics, University of New South Wales, Sydney, NSW 2052, Australia

Joseph P. Ndenda, Mary R. Myerscough

School of Mathematics and Statistics, University of Sydney, Carslaw Building, Eastern Avenue, Camperdown, Sydney, NSW 2006, Australia

Helen M. Byrne

Wolfson Centre for Mathematical Biology, Mathematical Institute, Andrew Wiles Building, University of Oxford, Woodstock Road, Oxford, Oxfordshire OX2 6GG, UK; and  
Ludwig Institute for Cancer Research, University of Oxford, Old Road Campus Research Build, Roosevelt Dr, Headington, Oxford, Oxfordshire, OX3 7DQ, UK

## 1 Introduction

Macrophages are a crucial cell type in the innate immune system. They are highly plastic cells that ingest pathogens and cellular debris, produce immune signals and promote healing. They exhibit a variety of phenotypes, some inflammatory and others anti-inflammatory. Macrophages are not only implicated in atherosclerosis [2] but also other inflammatory diseases such as chronic obstructive pulmonary disease [3], Alzheimer's disease [4], kidney disease [5] and cancer [6, 7].

Macrophages drive the growth of atherosclerotic plaque through inflammatory signalling, phagocytosis (ingestion) of modified low density lipoproteins (mod LDL) and efferocytosis (ingestion and removal) of apoptotic cells [2, 8]. They accumulate internalised lipid (mostly cholesterol) via phagocytosis of modLDL and efferocytosis of dead (apoptotic) cells, including their lipid membranes. Lipid-laden macrophages are usually described as foam cells since the accumulated internalised lipid gives them foamy appearance under the microscope. If a foam cell becomes apoptotic, then when it is ingested by another macrophage, its internalised lipid is added to the internalised lipid of the ingesting cell. In this way, macrophages can become very heavily lipid-laden. In a nascent atherosclerotic plaque, intercellular lipid accumulation via macrophage efferocytosis can drive the formation of necrotic regions in the plaque and cause the plaque to become increasingly pathological.

Macrophage efferocytosis in atherosclerotic plaques cannot be directly observed *in vivo*. *In vitro* experiments however shed useful light on how internalised lipid accumulates in plaque macrophages. Ford *et al* [1] performed experiments using latex microbeads to monitor the accumulation of apoptotic cell contents via efferocytosis.

Populations of macrophages were plated onto microscope slides after treatment with interferon  $\gamma$  (IFN $\gamma$ ) and lipopolysaccharide (LPS) to activate an inflammatory, efferocytic phenotype. Before the IFN $\gamma$  and LPS treatment, macrophages were incubated with latex beads at a ratio of approximately one bead per macrophage. Hence the expected number of beads per macrophage at the start of the experiment was one. As the experiment progressed, some macrophages became apoptotic and were ingested or engulfed by living macrophages, along with any beads that were contained in the apoptotic macrophage. Some bead-carrying macrophages underwent proliferation. When this occurred beads were divided between the daughter cells, although not necessarily equally.

Panel A of Fig. 1 shows micrographs of bead-containing macrophages, at the start of the experiment, after 24 [hr] and after 40 [hr]. Initially, macrophages contained between zero and three beads each. By 24 [hr] most macrophages have acquired more beads and there are fewer macrophages in the field of view. After 48 [hr] macrophages are heavily laden with beads, but some beads are not contained in cells which suggests that efferocytosis has started to become defective [8].

Panel B, Fig. 1, shows two cells at  $t = 0$ . The right hand cell undergoes apoptosis ( $t = 8$  [hr]) and is engulfed by the cell on the left ( $t = 16$  [hr]). Panel C shows an example of cell division. The cell in the centre at  $t = 0$  divides to give two daughter cells ( $t = 8$  [hr]). These daughter cells, in turn, each divide, the right one at  $t = 12$  [hr] and the left one at  $t = 24$  [hr].

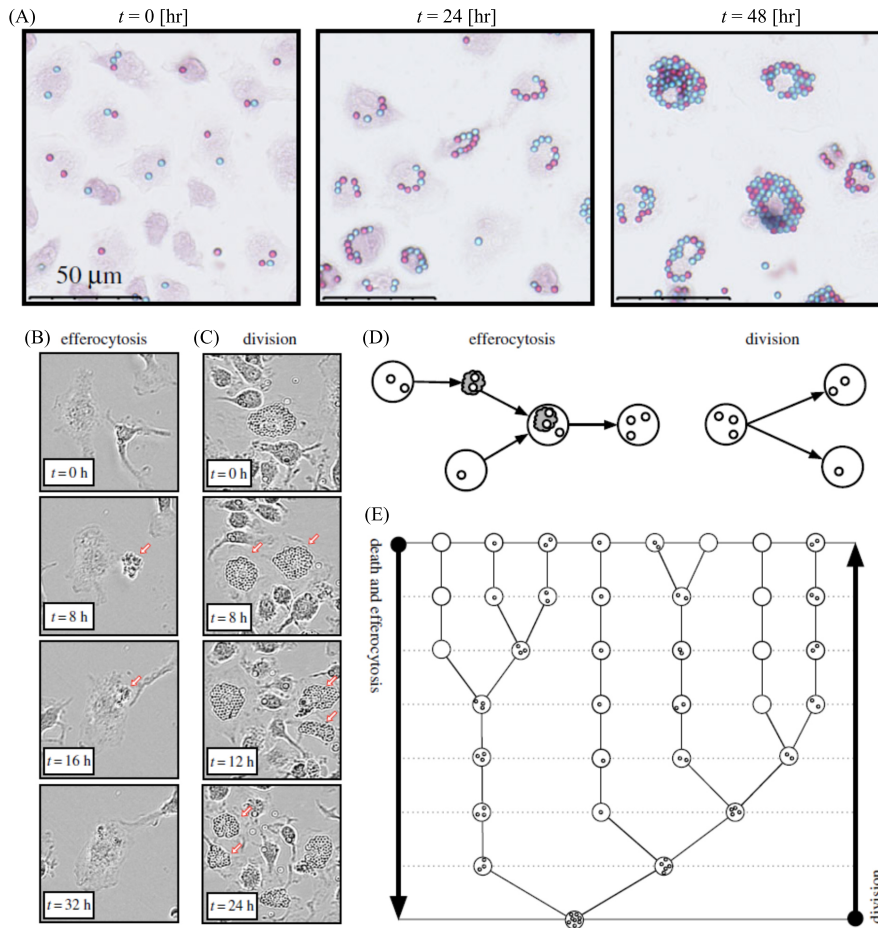


**Fig. 1: An *in-vitro* experiment to quantify bead accumulation inside a cannibalistic macrophage population.** (A) Experimental images showing bead accumulation in macrophages. (B) Experimental images showing redistribution of beads during macrophage apoptosis (during times 0 and 8 [hr]) and efferocytosis (during 16 and 32 h). (C) Experimental images showing redistribution of beads during macrophage division of one cell (during 0 and 8 [hr]) and of both daughter cells (during 8 and 12 [hr], and 12 and 24 [hr]). (D-E) Schematics showing the role of efferocytosis, cell death, and cell division on bead accumulation. Panel (A) reproduced from Figure 3A in [1] (CC BY 4.0). Panels (B)-(E) reproduced from Figure 1 from in [1] (CC BY 4.0).

Panel D, Fig. 1 shows schematics of bead accumulation via efferocytosis and bead distribution via proliferation for a pair of cells, while Panel E shows these processes on a population level. Panel E can either be read with time running from

top to bottom to describe accumulation via efferocytosis, or it can be read from bottom to top to describe distribution of beads via cell division.

Image analysis was used to determine the number of macrophages in the bead experiment and the number of beads in each macrophage at  $t = 0$ ,  $t = 24$  [hr] and  $t = 48$  [hr]. A plot of macrophage populations is given in Fig. 4(a) in the supplementary material of [1]. Ford *et al* [1] fitted an exponential curve to the data by eye and estimated that the average death rate at  $1/60$  [ $\text{h}^{-1}$ ]. They assumed that proliferation was negligible in this experiment.

In this paper we revisit the simple exponential model, assess it for model identifiability and then re-examine its fit to synthetic and experimental data using objective statistical parameter estimation and prediction techniques.

## 2 Data

We re-digitise previously published data from Figure 3 in [1]. The published data were generated from *in vitro* experiments designed to quantify the accumulation of latex beads, each of diameter  $3\ \mu\text{m}$ , within primary murine bone marrow-derived macrophage cells. In the experiment,  $10^5$  beads were incubated with  $10^5$  macrophage cells. The cells were then stimulated into an inflammatory state using interferon  $\gamma$  (IFN $\gamma$ ) and lipopolysaccharide (LPS). The number of beads per cell was counted for every cell using an image recognition algorithm applied to whole-slide photomicrographs. The total number of cells and the proportion of cells with  $n$  beads per cell were computed at times 0, 24, and 48 [hr], where time 0 [hr] corresponds to immediately prior to stimulation with IFN $\gamma$  and LPS. While the published data represent averages from four experiments performed with macrophages derived from different mice on different days, we do not have access to these data at present. From the re-digitised data describing the total number of cells, we obtain three measurements at each time point which correspond to the lower, central, and upper points from Figure 3B in [1]. For the re-digitised data for the number of beads per cell, for each timepoint we obtain at most one measurement for each possible value of number of beads per cell from Figure 3D in [1].

## 3 Methods

### 3.1 General mathematical model

Following [1], we consider an ordinary differential equation-based mathematical model that captures the key processes in the experiment: apoptosis (a form of cell death), efferocytosis (where one cell consumes another dead cell), and division (where a parent cell divides into two daughter cells). The total number of beads is

conserved throughout these processes. The redistribution of beads within the living and apoptotic macrophage cells may then be viewed as a coagulation–fragmentation process [9, 10]. Following [1], the number density of living macrophage cells containing  $n$  beads at time  $t$  [hr] is denoted  $\phi_n(t)$  [-], and the number density of apoptotic macrophage cells at time  $t$  [hr] containing  $n$  beads is denoted  $\phi_n^\dagger(t)$  [-]. The governing equations for the densities of the living and apoptotic cells are,

$$\begin{aligned} \frac{d\phi_n(t)}{dt} = & \underbrace{\eta \sum_{i=0}^n \phi_i^\dagger(t) \phi_{n-i}(t)}_{\text{efferocytosis source}} - \underbrace{\eta \phi_n(t) \sum_{i=0}^{\infty} \phi_i^\dagger(t)}_{\text{efferocytosis sink}} - \underbrace{\beta \phi_n(t)}_{\text{apoptosis sink}} \\ & + \underbrace{2\alpha \sum_{i=n}^{\infty} \binom{i}{n} \frac{\phi_i(t)}{2^i}}_{\text{division source}} - \underbrace{\alpha \phi_n(t)}_{\text{division sink}}, \end{aligned} \quad (1)$$

$$\frac{d\phi_n^\dagger(t)}{dt} = \underbrace{-\eta \phi_n^\dagger(t) \sum_{i=0}^{\infty} \phi_i(t)}_{\text{efferocytosis sink}} + \underbrace{\beta \phi_n(t)}_{\text{apoptosis source}}, \quad (2)$$

where  $\alpha$  [ $\text{hr}^{-1}$ ] is the cell division rate,  $\beta$  [ $\text{hr}^{-1}$ ] is the apoptosis rate, and  $\eta$  [ $\text{hr}^{-1}$ ] is the efferocytosis rate.

The total number of living macrophage cells,  $N(t)$ , and the total number of apoptotic macrophage cells,  $N^\dagger(t)$ , are given by,

$$N(t) = \sum_{i=0}^{\infty} \phi_i(t) \quad \text{and} \quad N^\dagger(t) = \sum_{j=0}^{\infty} \phi_j^\dagger(t). \quad (3)$$

### 3.2 Mathematical model with no cell division and instantaneous efferocytosis

Following [1], we assume that the impact of cell division is negligible in this experiment, and therefore we fix  $\alpha = 0$  in Eqs. (1)-(2). We also assume that apoptotic cells are instantaneously consumed, corresponding to  $\eta \rightarrow \infty$  in Eqs. (1)-(2) (see Supplementary Material of [1] for further details). Under these assumptions, the total number of live cells at time  $t$  is

$$N(t) = N(0) \exp(-\beta t), \quad (4)$$

where  $N(0)$  [-] is the initial number of living cells that we treat as a model parameter and  $\beta$  [ $\text{hr}^{-1}$ ] is the rate of apoptosis. These two parameters are globally structurally identifiable meaning that each parameter can be uniquely identified given continuous noise-free observations of  $N(t)$  [11]. This can be shown by taking the logarithm of Eq. (4) to obtain a line. From this line one can determine  $N(0)$  and  $\beta$  from the

vertical intercept and gradient, respectively. In what follows, we will explore if these parameters can be estimated given finite noisy data.

### 3.3 Statistical parameter estimation, identifiability analysis, and prediction

We use statistical modelling to connect the mathematical model in Eq. (4) to the experimental data. The experimental data that we focus on comprise three measurements of the total number of living cells at three times  $t_i = 0, 24, 48$  [hr]. We assume that at each time  $t_i$  each experimental observation  $j$ , denoted  $N_{i,j}^o$ , is distributed about the mathematical model solution  $N(t_i; N(0), \beta)$  that depends on the values of  $N(0)$  and  $\beta$ . Specifically, we assume that

$$N_{i,j}^o \sim \mathcal{N}(N(t_i; N(0), \beta), \sigma), \quad (5)$$

where  $\mathcal{N}(\mu, \sigma)$  represents a Gaussian probability distribution with mean  $\mu$  and standard deviation  $\sigma$ . This assumption of additive Gaussian noise, also often referred to as normally distributed noise, is widely used in the literature and appears appropriate for this preliminary analysis [12]. We denote the entire dataset with  $N_{1:9}^o = \{N_{i,j}^o \mid i \in \{1, 2, 3\}, j \in \{1, 2, 3\}\}$ . In this report, we estimate the mathematical model parameters,  $N(0)$  and  $\beta$ , and the statistical model parameter,  $\sigma$ , from the data simultaneously.

To estimate the mathematical and statistical model parameters,  $\theta = (\beta, N(0), \sigma)$ , we employ an established profile likelihood-based workflow for statistical parameter estimation, practical identifiability analysis, and prediction [12]. Throughout we work with the log-likelihood function,

$$\ell(\theta \mid N_{1:9}^o) = \sum_{i=1}^3 \sum_{j=1}^3 \log \left[ \phi \left( N_{i,j}^o; N(t_i; N(0), \beta), \sigma \right) \right], \quad (6)$$

where  $\phi(x; \mu, \sigma)$  is the Gaussian probability density function with mean  $\mu$  and standard deviation  $\sigma$ .

The maximum likelihood estimate (MLE) is then

$$\hat{\theta} = \underset{\theta}{\operatorname{argmax}} \ell(\theta \mid N_{1:9}^o). \quad (7)$$

Under the assumption of additive Gaussian noise, the mathematical model solution evaluated at the MLE is the best match to the data, in the sense of the highest likelihood, and is identical to the mathematical model solution obtained via the routinely employed method of least squares.

There may be a range of values of  $\theta$  that result in similar agreement to the data as the MLE. To determine this range of values, we use an established profile likelihood-based approach detailed in [12]. In particular, we compute profile likelihoods work-

ing with the normalised log-likelihood,

$$\hat{\ell}(\boldsymbol{\theta} | N_{1:9}^o) = \ell(\boldsymbol{\theta} | N_{1:9}^o) - \ell(\hat{\boldsymbol{\theta}} | N_{1:9}^o), \quad (8)$$

such that  $\hat{\ell}(\boldsymbol{\theta} | N_{1:9}^o) \leq 0$  and  $\hat{\ell}(\hat{\boldsymbol{\theta}} | N_{1:9}^o) = 0$ . From these profiles, we compute an approximate 95% confidence interval for each parameter in  $\boldsymbol{\theta}$  in turn. If an approximate confidence interval is narrow relative to pre-specified parameter bounds, we refer to the parameter as being *practically identifiable*. Otherwise, we refer to the parameter as being *practically non-identifiable*. Informed by experimental observations, and preliminary explorations, we set the following parameter bounds  $0.00 \leq \beta \leq 0.05$  [ $\text{hr}^{-1}$ ],  $8 \times 10^4 \leq N(0) \leq 12 \times 10^4$  [-], and  $100 \leq \sigma \leq 2 \times 10^4$  [-]. As the mathematical model parameters in this study are structurally identifiable, if we observe that a parameter is practically non-identifiable this suggests that additional observations are required to recover practical identifiability of the model parameters. We also propagate forward the uncertainty in the approximate confidence intervals for the model parameters to generate profile-wise confidence sets for deterministic model solutions and profile-wise confidence sets for noisy data realisations (method detailed in [12]).

## 4 Results

We quantify bead accumulation inside a cannibalistic macrophage population using *in vitro* experimental data, mathematical modelling, and statistical modelling. As described in the mathematical and statistical methods (Section 3), a key parameter that characterises bead accumulation dynamics is the rate of apoptosis,  $\beta$ . Two additional parameters capture the initial number of living cells,  $N(0)$ , and statistical noise,  $\sigma$ . Before analysing the experimental data we perform a synthetic data study to verify that the method accurately recovers known parameters. We then analyse the experimental data and compare our new objective parameter estimates to previously reported values that were obtained via visual inspection.

### 4.1 Synthetic data

To verify that our methods recover known parameters, we perform a synthetic data study. We simulate the mathematical model in Eq. (4) using the values reported in [1], specifically  $N(0) = 8 \times 10^4$  [-] and  $\beta = 1/60 = 0.0167$  [ $\text{hr}^{-1}$ ]. We generate three independent observations at each of three time points,  $t = 0, 24, 48$  [hr], and set  $\sigma = 10^4$  [-]. By definition, these synthetic data display an exponential decrease in total cell number with time (Fig. 2A). We then compute the MLE,  $\hat{\boldsymbol{\theta}} = (\hat{\beta}, \hat{N}(0), \hat{\sigma}) = (0.0139, 8.02 \times 10^4, 8.03 \times 10^3)$ , and find that it is close to the known values used to generate the synthetic data. Evaluating the mathemati-

cal model in Eq. (4) at the MLE we observe good agreement to the synthetic data (Fig. 2A). We then generate profile likelihoods for each model parameter (Fig. 2B-D). As each profile likelihood is unimodal and narrow relative to the pre-specified bounds, we conclude that each parameter is practically identifiable. The approximate 95% confidence intervals also capture the known parameter values used to generate the data. Profile-wise confidence sets for deterministic model solutions demonstrate how uncertainty in parameter estimates influences predictions (Fig. 3A-D) and profile-wise confidence sets for noisy data realisations show good agreement with the synthetic data (Fig. 3E-H).

The study in [1] also reports another key quantity: the distribution of the number of beads per cell. We now show how we can use our fitted value for  $\beta$  to predict the distribution of the number of beads per cell. We assume that the initial distribution of beads per cell,  $\phi_n(t=0)$  for  $n = 1, 2, \dots, n_{\max}$ , is known from the experimental data. We also assume that the maximum number of beads that can be contained in any single living or apoptotic cell is  $n_{\max} = 100$ . The structured mathematical model in Eqs. (1)-(2) then reduces to  $2n_{\max} + 2$  ordinary differential equations, each involving finite, rather than infinite, sums. A simulation of the structured model with the same known value of  $\beta = 1/60$  [hr], and  $\alpha = 0$ ,  $\eta = 10^4$  is shown in Fig. 4.

We next explore how the uncertainty in the approximate confidence interval for  $\beta$ , obtained from the analysis of synthetic data for the total number of living cells, influences predictions of the distribution of beads per cell. These predictions, in the form of confidence sets for the deterministic model solution of the structured model, are in good agreement with the simulated data (Fig. 4). We do not generate confidence sets for noisy data realisations of the structured model as it is not immediately clear how to attribute the population-level statistical noise,  $\sigma$ , to each compartment,  $\phi_n(t)$  for  $n = 0, 1, \dots, n_{\max}$ , of the structured mathematical model.

## 4.2 Experimental data

We now analyse the experimental data using the same workflow as in the synthetic data study. The MLE is found to be  $\hat{\theta} = (\hat{\beta}, N(0), \hat{\sigma}) = (0.0231, 9.2 \times 10^4, 6.0 \times 10^3)$ . Simulating the mathematical model with the MLE we observe good agreement to the experimental data describing the total number of cells (Fig. 5A). The profile likelihoods suggest that all parameters are practically identifiable (Fig. 5B-D).

Previous work analysing the raw experimental data estimated  $\beta = 0.0167$  [hr<sup>-1</sup>] via visual inspection [1]. This estimate is not contained within the approximate 95% confidence interval for  $\beta$  that we obtain by analysing the re-digitised data. The previously reported value for  $N(0)$  from [1] is also not contained within the corresponding approximate 95% confidence interval. Simulating the mathematical model at the values considered in [1] we observe poor agreement with the experimental data (Fig 5A). Our improved results are due to the objective statistical framework that we employ for parameter estimation. However, we caution that we have analysed the

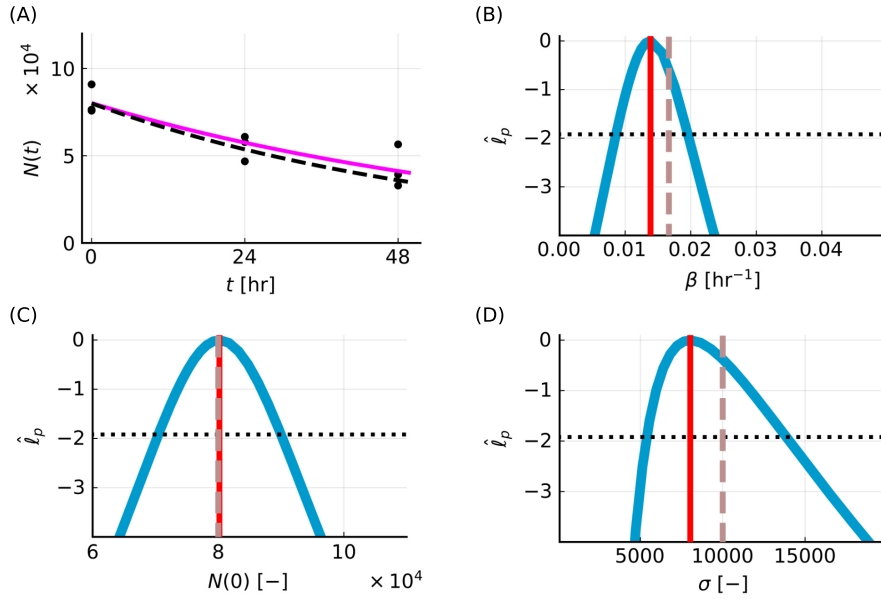


**Fig. 2: Best-fit and profile likelihoods for synthetic data study** (A) Synthetic data (circles) generated by simulating the mathematical model in Eq. (4) with additive Gaussian noise with known parameters,  $\theta = (\beta, N(0), \sigma) = (0.0167, 8 \times 10^4, 10^4)$ , Simulation of the mathematical model in Eq. (4) evaluated at the known parameters (black dashed line) and at the MLE (magenta solid line),  $\hat{\theta} = (\hat{\beta}, N(\hat{0}), \hat{\sigma}) = (0.0139, 8.02 \times 10^4, 8.03 \times 10^3)$ . (B-D) Profile likelihoods (blue) for (B)  $\beta$ , (C)  $N(0)$ , (D)  $\sigma$  with MLE (vertical red dashed), known parameters (vertical brown dashed) an approximate 95% confidence interval threshold (horizontal black-dashed). Approximate 95% confidence intervals:  $0.0101 \leq \beta \leq 0.0190$ ,  $9.0 \times 10^4 \leq N(0) \leq 1.1 \times 10^4$ , and  $5.4 \times 10^3 \leq \sigma \leq 13.9 \times 10^3$ .

re-digitised data rather than the raw data. Analysing the raw data may yield results that are closer to the previously reported values.

Profile-wise confidence sets for deterministic model solutions reveal how uncertainty in parameter estimates influences predictions (Fig. 6A-D) and profile-wise confidence sets for noisy data realisations show good agreement with the experimental data (Fig. 6E-H). These results are consistent with the synthetic data study.

We next propagate the uncertainty in  $\beta$  to generate predictions of the distribution of beads per cell. These predictions, in the form of confidence sets for the deterministic model solution of the structured model, demonstrate good agreement with the experimental data for most cells (Fig. 6). We observe discrepancies between the simulation of the structured mathematical model and the experimental data for a small proportion of cells that contain many beads. This discrepancy is not unexpected as we compare experimental data to a confidence set for the model solution. It would

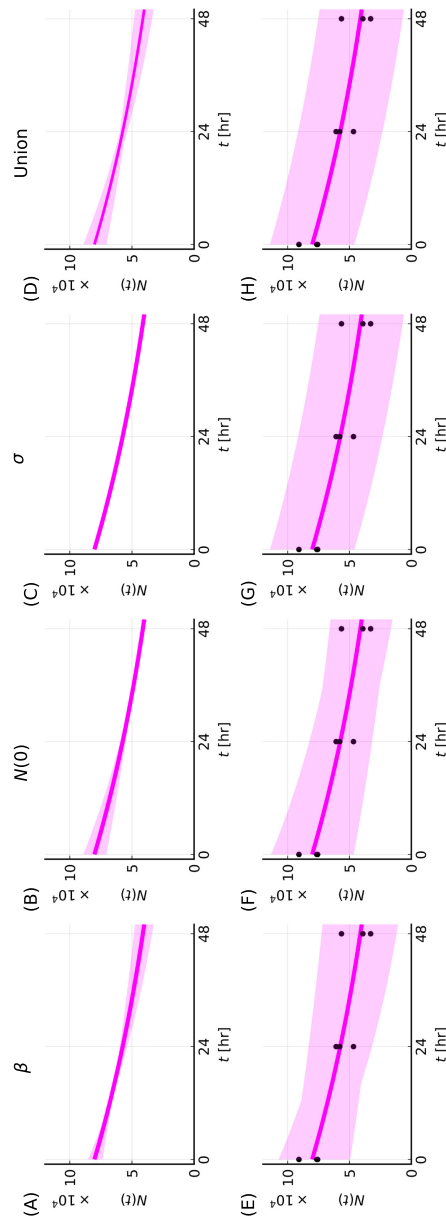


**Fig. 3: Predictions for  $N(t)$  in the synthetic data study.** (A-C) Profile-wise confidence sets for deterministic model solutions for (A)  $\beta$ , (B)  $N(0)$ , and (C)  $\sigma$ . (D) Union of profile-wise confidence sets in (A-C). (E-G) Profile-wise confidence sets for noisy data realisations (E)  $\beta$ , (F)  $N(0)$ , and (G)  $\sigma$ . (H) Union of confidence sets for noisy data realisations from (E-G).

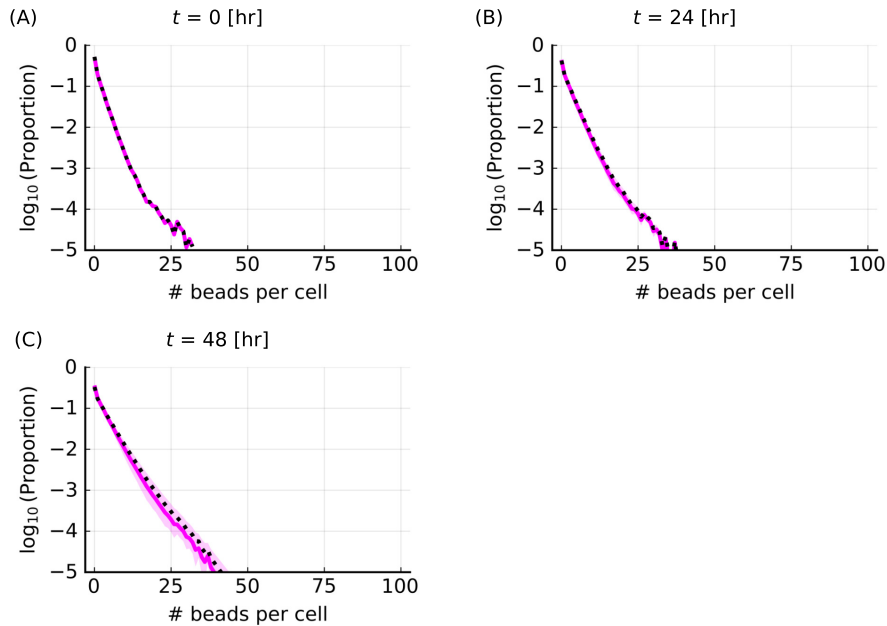


**Fig. 4: Predictions for distribution of the number of beads per cell for synthetic data study.** Simulation of the structured mathematical model from Eqs. (1)-(2) evaluated at the known value of  $\beta = 0.0167$  [hr<sup>-1</sup>] (black dotted line) and at the MLE  $\beta = 0.0139$  (solid magenta). Initial condition at  $t = 0$  [hr] set equal to experimental data. Approximate 95% confidence set for the distribution of the number of beads per cell (magenta shaded).

be more sensible to compare the experimental data to a confidence set for noisy data realisations of the structured mathematical model. However, it is unclear which statistical error model should be applied to the structured mathematical model and how this connects to the estimated population-level statistical noise,  $\sigma$ .

## 5 Discussion

In this study, we quantify bead accumulation inside a cannibalistic population of macrophages. We used an existing ordinary differential equation-based mathematical model designed to quantify the accumulation of latex beads within macrophages [1], and made some simplifying assumptions about cell division and efferocytosis. We then applied a profile likelihood-based parameter estimation, practical identifiability analysis, and prediction workflow using synthetic data (Section 4.1) and then using re-digitised published data from Figure 3 in [1] (Section 4.2). The results for the synthetic data demonstrate good agreement with the simulated data (Figs. 2–4),

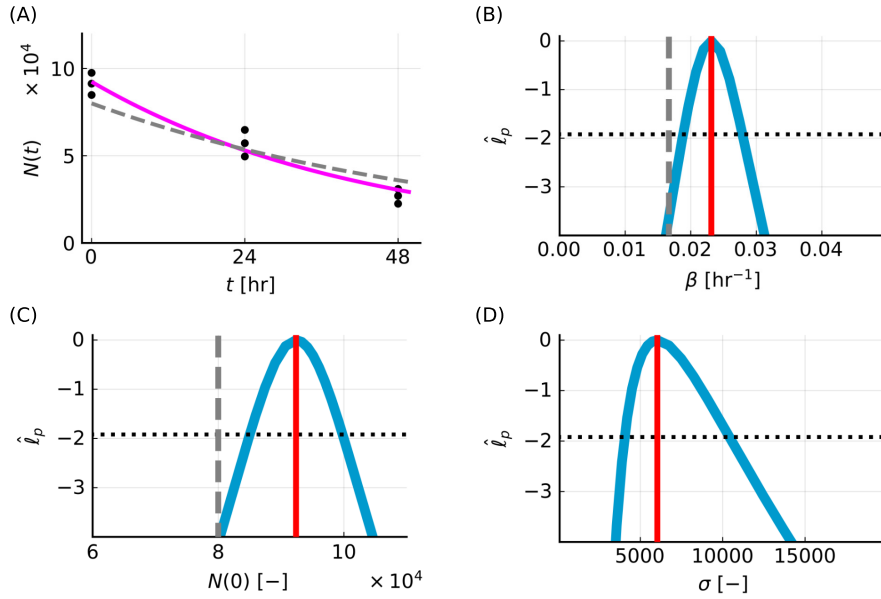


**Fig. 5: Best-fit and profile likelihoods for experimental data** (A) Experimental data (circles), simulation of the mathematical model in Eq. (4) evaluated at values considered in [1],  $(\beta, N(0)) = (0.0167, 8 \times 10^4)$  (grey dashed), and at the MLE (magenta solid line),  $\hat{\theta} = (\hat{\beta}, N(\hat{0}), \hat{\sigma}) = (0.0231, 9.2 \times 10^4, 6.0 \times 10^3)$ . (B–D) Profile likelihoods (blue) for (B)  $\beta$ , (C)  $N(0)$ , (D)  $\sigma$  with MLE (vertical red dashed), values considered in [1] (vertical grey dashed), and an approximate 95% confidence interval threshold (horizontal black-dashed). Approximate 95% confidence intervals:  $0.0189 \leq \beta \leq 0.0279$ ,  $8.5 \times 10^4 \leq N(0) \leq 10.0 \times 10^4$ , and  $4.1 \times 10^3 \leq \sigma \leq 10.4 \times 10^3$ .

giving us confidence to apply the workflow to the re-digitised data (Figs. 5–7). Results for the digitised data show that the reported value of  $\beta$  from [1] is outside of the approximate confidence interval obtained in this analysis.

There are many future directions for the work presented here. Firstly, the error model we have adopted in this work for the population size of living cells at time  $t$  is a normal distribution, which has infinite support; this is not biologically realistic. The assumption could be relaxed to use a distribution with positive support, for example a log-normal distribution. Secondly, following [1], we assume that the role of cell division is negligible by setting  $\alpha = 0$  in Eqs. (1)–(2). The work presented here could be extended to consider non-zero cell proliferation; this would complicate the underlying dynamical system but the statistical parameter estimation, identifiability analysis and prediction process would proceed as presented here. At the scale of the total cell number, additional types of data would be required to decouple the proliferation rate,  $\alpha$ , and the rate of apoptosis,  $\beta$ . In the same vein, we could consider the

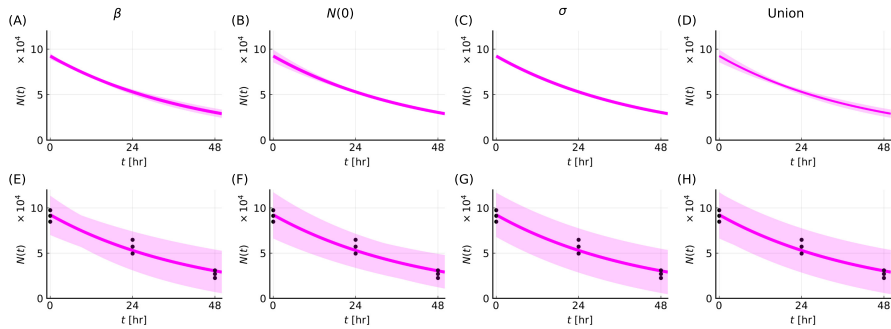


**Fig. 6: Predictions for  $N(t)$  when analysing experimental data.** (A-C) Profile-wise confidence sets for deterministic model solutions for (A)  $\beta$ , (B)  $N(0)$ , and (C)  $\sigma$ . (D) Union of profile-wise confidence sets in (A-C). (E-G) Profile-wise confidence sets for noisy data realisations (E)  $\beta$ , (F)  $N(0)$ , and (G)  $\sigma$ . (H) Union of confidence sets for noisy data realisations from (E-G).

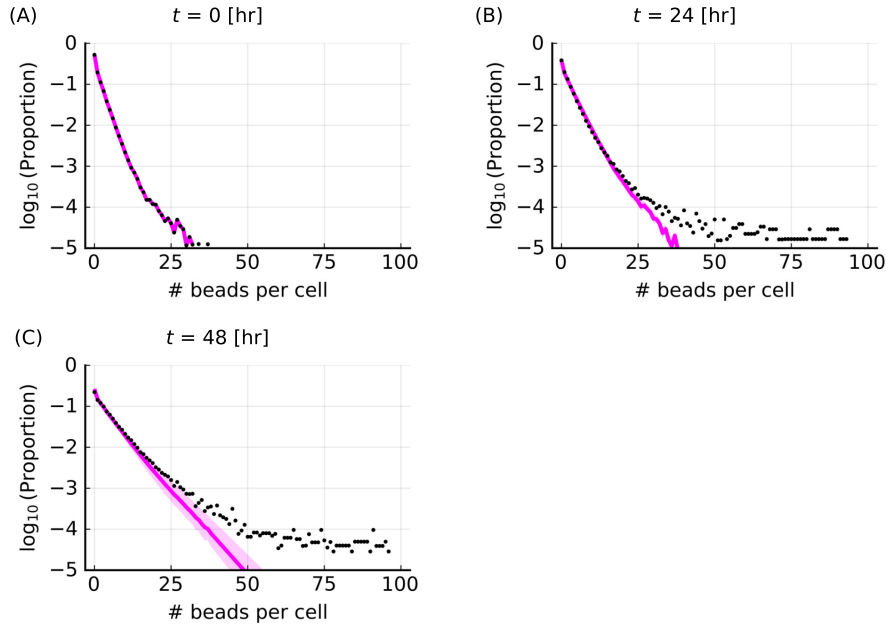


**Fig. 7: Predictions for distribution of the number of beads per cell for experimental data.** (A-C) Experimental data (black circles) and simulation of the structured mathematical model from Eqs. (1)-(2) evaluated at the MLE  $\beta = 0.0231$  (solid magenta). Initial condition at  $t = 0$  [hr] set equal to experimental data. Approximate 95% confidence set for the distribution of the number of beads per cell (magenta shaded).

model under various, finite, values for the rate of efferocytosis,  $\eta$ . The original paper by Ford *et al.* [1] presented additional data on the lipid content of the macrophages that we have not used but that could be incorporated into the workflow presented here. In the analysis of experimental data we work with re-digitised data from [1]. This re-digitised data is a representation of the raw data. It would be interesting to revisit this analysis using the complete raw data. A final avenue for future work is to design a single inference framework that uses both the total number of cells at each time point and the number of beads per cell; this would require data integration techniques to construct a joint observational model and hence joint likelihood function for both sets of data.

While there are several limitations to the approach developed here, this report presents a first step to formal calibration and identifiability analysis of an existing model and dataset in the literature of bead accumulation inside macrophages. Our analysis is a useful basis for future studies exploring lipid content in macrophages.

### Data and code availability

Re-digitised data and key Julia code that we use to perform this analysis are available on a GitHub repository (<https://github.com/ryanmurphy42/Murphy2024AtheroAnnals>).

**Acknowledgements** We thank the mathematical research institute MATRIX in Australia, where this research was performed as part of the MATRIX Research Program: Mathematical Models for Lipids and Cells in Atherosclerotic Plaques.

### References

- [1] Ford HZ, Zeboudj L, Purvis GS, ten Bokum A, Zarebski AE, Bull JA, Byrne HM, Myerscough MR, Greaves DR. (2019). Efferocytosis perpetuates substance accumulation inside macrophage populations. *Proceedings of the Royal Society B*. 286(1904), 20190730. (doi:10.1098/rspb.2019.0730).
- [2] Lusis AJ. (2000) Atherosclerosis. *Nature*. 407, 233–241. (doi:10.1038/35025203).
- [3] Vlahos R, Bozinovski S. (2014). Role of alveolar macrophages in chronic obstructive pulmonary disease. *Frontiers in Immunology*. 5, 435. (doi:10.3389/fimmu.2014.00435).
- [4] Mammanna S, Fagone P, Cavalli E, Basile MS, Petralia MC, Nicoletti F, Bramanti P, Mazzon E. (2018). The role of macrophages in neuroinflammatory and neurodegenerative pathways of Alzheimer’s disease, amyotrophic lateral sclerosis, and multiple sclerosis: pathogenetic cellular effectors and potential therapeutic targets. *International Journal of Molecular Sciences*. 19(3), 831. (doi:10.3390/ijms19030831).
- [5] Wen Y, Crowley SD. (2020). The varying roles of macrophages in kidney injury and repair. *Current Opinion in Nephrology and Hypertension*. 29(3), 286-292. (doi:10.1097/MNH.0000000000000595).
- [6] Zhou L, Zhao T, Zhang R, Chen C, Li J. (2024). New insights into the role of macrophages in cancer immunotherapy. *Frontiers in Immunology*. 15, 1381225. (doi:10.3389/fimmu.2024.1381225).

- [7] Zhang J, Hu C, Zhang R, Xu J, Zhang Y, Yuan L, Zhang S, Pan S, Cao M, Qin J, Cheng X, Xu Z. (2023). The role of macrophages in gastric cancer. *Frontiers in Immunology*. 14, 1282176. (doi:10.3389/fimmu.2023.1282176).
- [8] Tabas I. (2010). Macrophage death and defective inflammation resolution in atherosclerosis. *Nature Reviews Immunology*. 10(1), 36-46. (doi:10.1038/nri2675).
- [9] Aldous DJ. (1999). Deterministic and stochastic models for coalescence (aggregation and coagulation): a review of the mean-field theory for probabilists. *Bernoulli*. 1, 3–48. (doi:10.2307/3318611).
- [10] Bertoin J. (2006). Random fragmentation and coagulation processes. Cambridge, UK: Cambridge University Press.
- [11] Rey Barreiro X, Villaverde AF. (2023). Benchmarking tools for a priori identifiability analysis. *Bioinformatics*. 39(2), btad065. (doi:10.1093/bioinformatics/btad065).
- [12] Murphy RJ, Maclaren OJ, Simpson MJ. (2024). Implementing measurement error models with mechanistic mathematical models in a likelihood-based framework for estimation, identifiability analysis and prediction in the life sciences. *Journal of the Royal Society Interface*. 21(210), 20230402. (doi:10.1098/rsif.2023.0402).